

# Revista Mexicana de Astronomía y Astrofísica

Revista Mexicana de Astronomía y Astrofísica  
Universidad Nacional Autónoma de México  
rmaa@astroscu.unam.mx  
ISSN (Versión impresa): 0185-1101  
MÉXICO

2007

Xue-Guang Zhang / Deborah Dultzin Hacyan / Ting-Gui Wang  
THE PROPERTIES OF OPTICAL FEII EMISSION LINES OF AGN WITH DOUBLE-  
PEAKED BROAD EMISSION LINES (PARTE B)

*Revista Mexicana de Astronomía y Astrofísica*, año/vol. 43, número 001

Universidad Nacional Autónoma de México

Distrito Federal, México

pp. 111-121

Red de Revistas Científicas de América Latina y el Caribe, España y Portugal

Universidad Autónoma del Estado de México

<http://redalyc.uaemex.mx>



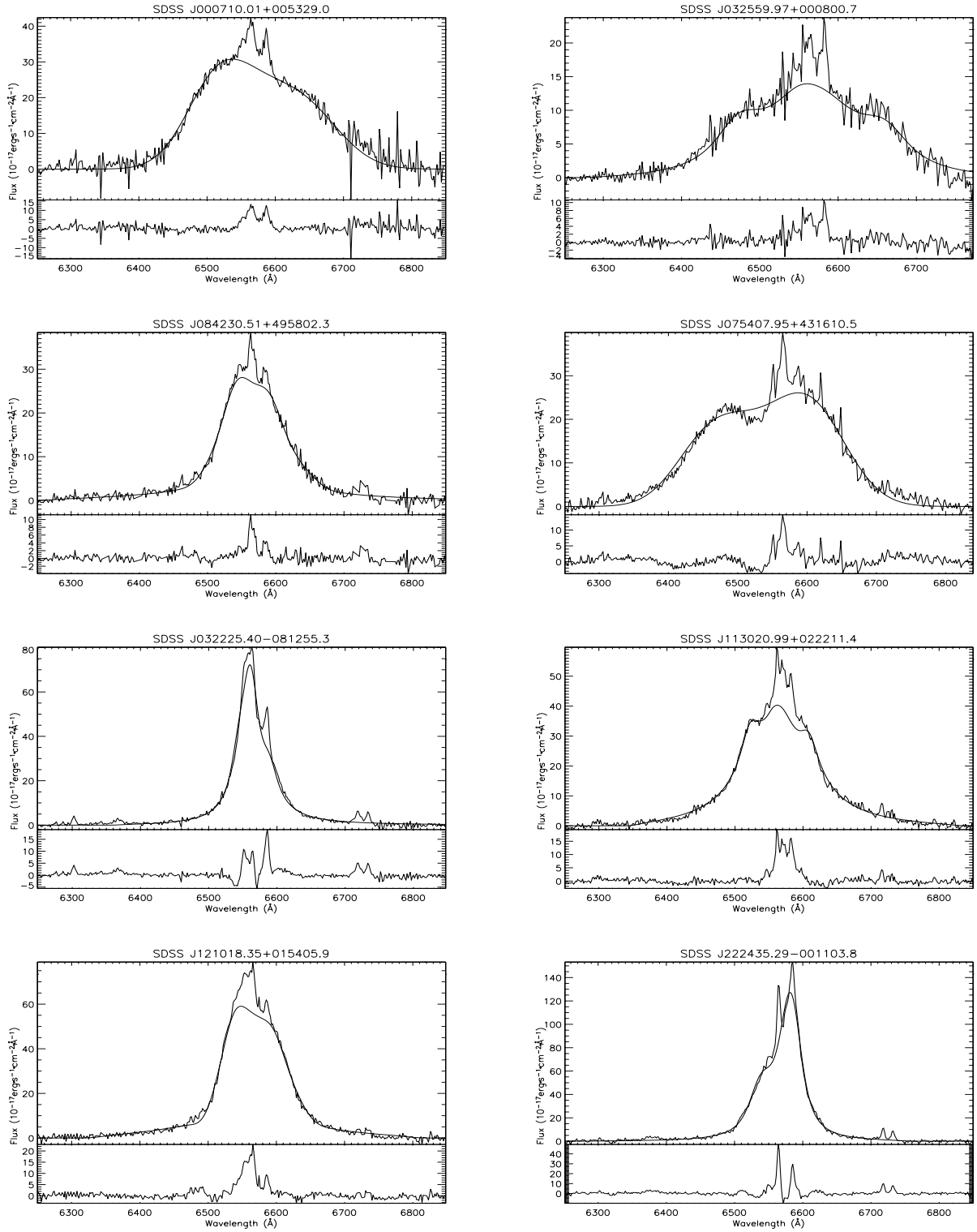


Fig. 3. The best fitted results for double-peaked broad  $H\alpha$ . The lower panel in each plot shows the spectrum after the subtraction of the broad  $H\alpha$  coming from the accretion disk. The model parameters are listed in Table 1.

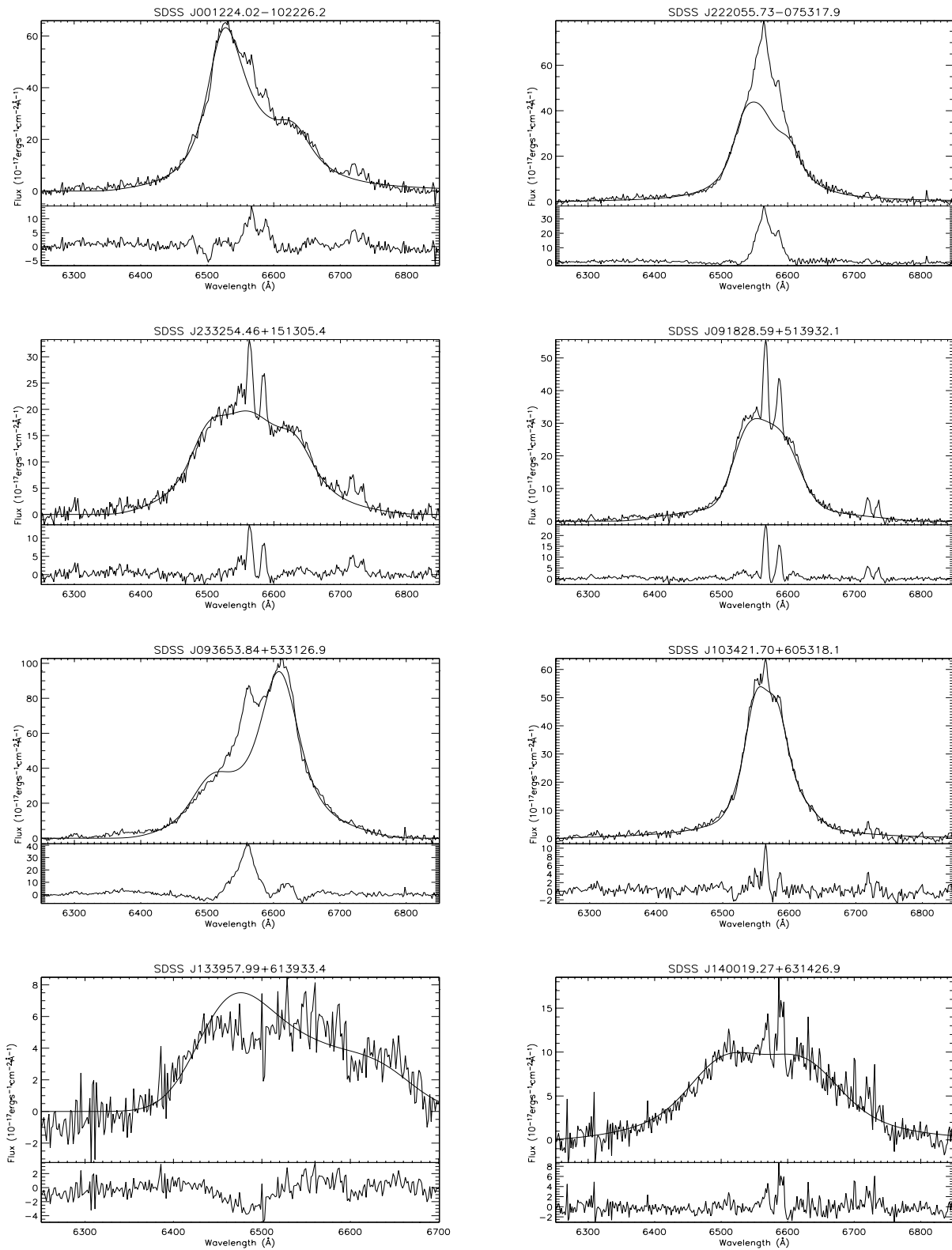


Fig. 3. Continued.

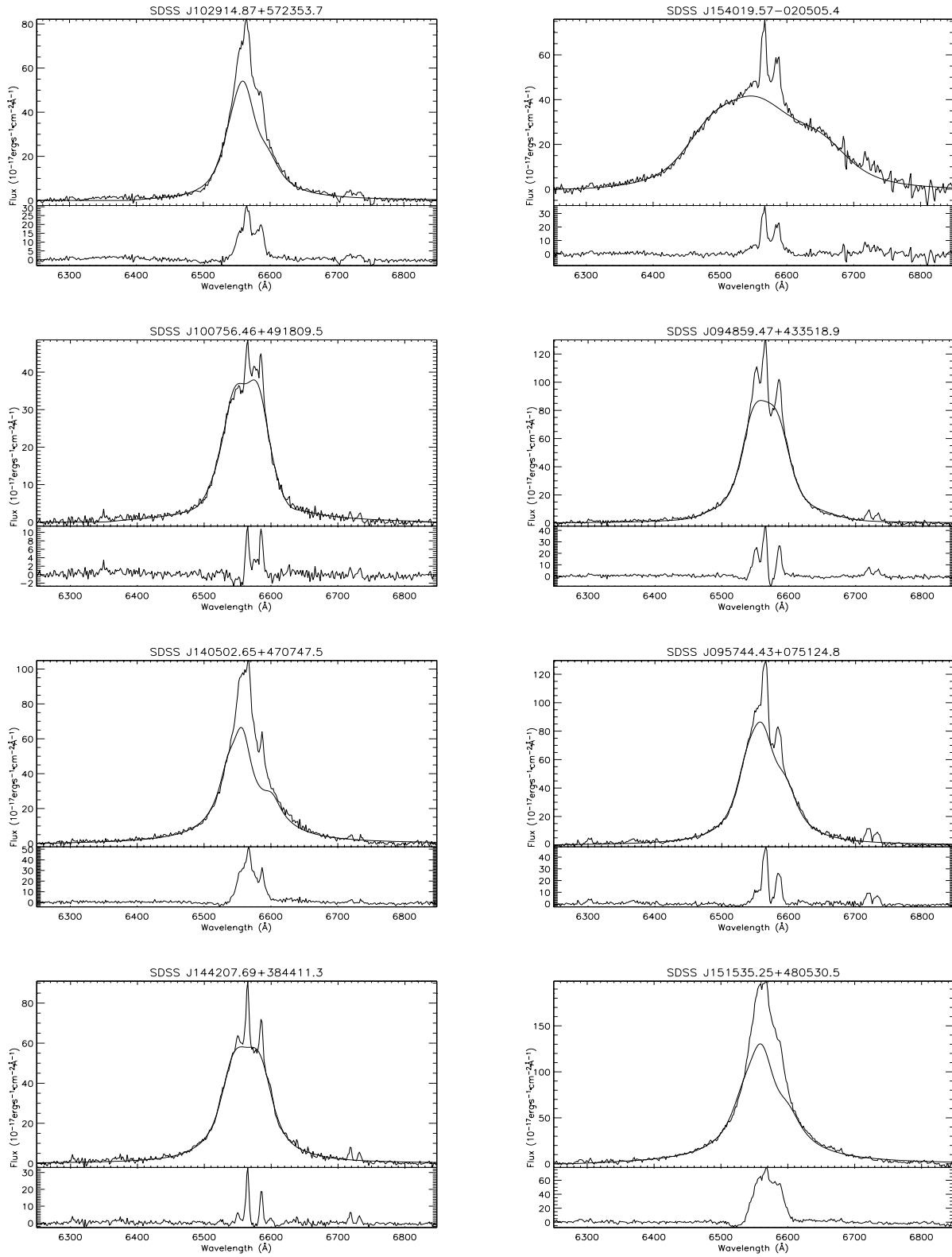


Fig. 3. Continued.

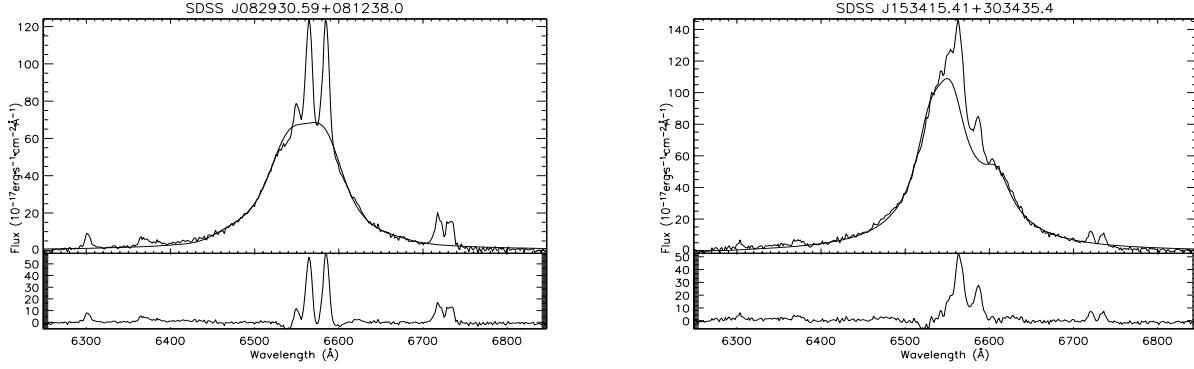


Fig. 3. Continued.

free parameters (MPFIT package in IDL). There are eight free parameters in the elliptical accretion disk model, the inner radius  $r_{in}$ , the outer radius  $r_{out}$ , the inclination angle of the accretion disk  $i$ , the local broadening velocity dispersion  $\sigma$ , the slope of the line emissivity  $q$ , the eccentricity  $e$ , the orientation angle of the accretion disk  $\phi_0$  and an amplitude factor  $k$ . The best fitted results are shown in Figure 3. The parameters of the accretion disk model for each dbp emitter are listed in Table 2.

We select an elliptical accretion disk model rather than a circular disk plus spiral arm model due to the following considerations. For the elliptical disk model, there are mainly five parameters to determine: the observed line profile,  $r_{in}$ ,  $r_{out}$ ,  $i$  and  $e$ . However, in the circular disk plus spiral arm model, there are another four parameters that dominate the observed line profile. To some extent, we think the uniqueness of the model parameters for an elliptical accretion disk model is better than that of the circular disk plus spiral arm model. Also, we do not select a simple circular accretion disk model because the model cannot be applied for dbp emitters which have a red peak brighter than the blue peak.

Last, we measure the line parameters of broad  $H\alpha$ , such as the line width of  $H\alpha$ ,  $\sigma_{H\alpha_B}$ . The line parameters of the broad component of  $H\alpha$  can be measured by:

$$\lambda_0 = \frac{\int \lambda f_\lambda d\lambda}{\int f_\lambda d\lambda}$$

$$\sigma_g^2 = \frac{\int \lambda^2 f_\lambda d\lambda}{\int f_\lambda d\lambda} - \lambda_0^2 = \frac{\int (\lambda - \lambda_0)^2 f_\lambda d\lambda}{\int f_\lambda d\lambda}.$$

We find that the mean value of  $f_\lambda$  after the subtraction of the continuum is zero for the nearby points on the continuum. However, the mean value  $(\lambda - \lambda_0)^2 f_\lambda$  for those points further out is not zero, and becomes larger for the points selected from more

extended distances from the center of the emission line, unless we use a smoother background after the subtraction of the continuum for which the value at each point is equal to zero. Thus, we should select cautiously the wavelength to measure the second moment according to the equation above. The wavelength range is selected as follows: after the subtraction of the continuum and the bad pixels, we select the last point for which the flux is equal to the minimum value of the points on the blue side of the emission line (sometimes, the minimum value of the flux is not equal to zero) and select the first point for which the flux is equal to the minimum value of the points on the red side of the emission line. Due to the composite nature of the line profile of double-peaked emission, we think it is more accurate to measure the second moment of the broad  $H\alpha$  using the equation above, than to measure the value of FWHM of  $H\alpha$  according to the standard definition of FWHM, because the flux density of the broad component is the largest one in the composite emission line after the subtraction of the narrow emission lines. The value of  $\sigma_{H\alpha_B}$  is listed in Table 1.

### 3.2. Properties of FeII emission lines of dbp emitters

First, we check the correlation between line width of broad Balmer emission lines and strength of FeII emission lines  $EW(\text{FeII})/EW(\text{H}\beta)$ . We show the correlation in Figure 4. The mean value of the second moment of broad  $H\alpha$  is about  $3002 \pm 139 \text{ km} \cdot \text{s}^{-1}$ . As pointed out above, we use the second moment of broad  $H\alpha$  rather than  $\text{FWHM}(H\alpha)$ . The Spearman Rank correlation coefficient is -0.39 with  $P_{null} \sim 5\%$ . Here, the data include the object SDSS J2125-0813, for which the second moment of broad  $H\alpha$  is estimated from the broad component of  $H\beta$  reproduced by the accretion disk model. The

TABLE 1  
DATA OF THE SAMPLE

| Id | Name                | $z$    | $m_r$ | $R$   | $\sigma_{[\text{OIII}]}$<br>$\text{km} \cdot \text{s}^{-1}$ | $\sigma_{H\alpha_B}$<br>$\text{km} \cdot \text{s}^{-1}$ | $\log(L_{5100\text{\AA}})$<br>$\text{erg} \cdot \text{s}^{-1}$ | $\log(M_{BH})$<br>$M_\odot$ | $\log(\dot{m})$ |
|----|---------------------|--------|-------|-------|-------------------------------------------------------------|---------------------------------------------------------|----------------------------------------------------------------|-----------------------------|-----------------|
| 0  | J000710.01+005329.0 | 0.3162 | 17.13 | 0.48  | 290.96±2.925                                                | 3414.60                                                 | 44.09                                                          | 8.78                        | -1.88           |
| 1  | J032559.97+000800.7 | 0.3609 | 17.88 |       | 241.56±4.854                                                | 3868.92                                                 | 44.62                                                          | 8.45                        | -1.02           |
| 2  | J075407.95+431610.5 | 0.3476 | 17.23 | 1.50  | 179.50±2.068                                                | 3718.52                                                 | 44.68                                                          | 7.94                        | -0.44           |
| 3  | J113020.99+022211.4 | 0.2411 | 17.51 | 0.45u | 325.12±4.467                                                | 3136.51                                                 | 44.15                                                          | 8.97                        | -2.01           |
| 4  | J001224.02-102226.2 | 0.2282 | 16.91 | 0.65  | 270.19±8.137                                                | 3375.07                                                 | 44.36                                                          | 8.65                        | -1.48           |
| 5  | J233254.46+151305.4 | 0.2147 | 17.23 |       | 193.32±2.888                                                | 3282.24                                                 | 44.13                                                          | 8.07                        | -1.12           |
| 6  | J091828.59+513932.1 | 0.1854 | 17.13 | 0.43  | 149.72±2.815                                                | 2632.22                                                 | 44.02                                                          | 7.62                        | -0.79           |
| 7  | J093653.84+533126.9 | 0.2280 | 16.86 | 0.53  | 266.58±3.254                                                | 2951.40                                                 | 44.35                                                          | 8.63                        | -1.46           |
| 8  | J133957.99+613933.4 | 0.3724 | 18.68 |       | 309.30±9.214                                                | 3363.38                                                 | 44.26                                                          | 8.89                        | -1.81           |
| 9  | J140019.27+631426.9 | 0.3314 | 17.76 | 0.55u | 255.49±13.13                                                | 4611.71                                                 | 44.44                                                          | 8.55                        | -1.30           |
| 10 | J154019.57-020505.4 | 0.3204 | 16.73 | 0.80  | 187.93±3.000                                                | 3953.81                                                 | 44.83                                                          | 8.02                        | -0.37           |
| 11 | J2125-0813          | 0.6239 | 17.07 | 0.46  | 268.29±12.57                                                | 5026.95                                                 | 45.21                                                          | 8.64                        | -0.61           |
| 12 | J084230.51+495802.3 | 0.3050 | 17.93 | 0.59u | 239.02±6.430                                                | 2780.96                                                 | 44.33                                                          | 8.44                        | -1.29           |
| 13 | J032225.40-081255.3 | 0.1260 | 17.96 |       | 141.04±3.522                                                | 2152.76                                                 | 43.59                                                          | 7.52                        | -1.11           |
| 14 | J121018.35+015405.9 | 0.2158 | 17.23 | 0.30u | 180.30±3.434                                                | 2617.29                                                 | 44.33                                                          | 7.94                        | -0.80           |
| 15 | J222435.29-001103.8 | 0.0581 | 17.05 |       | 152.92±4.589                                                | 1975.48                                                 | 43.26                                                          | 7.66                        | -1.58           |
| 16 | J103421.70+605318.1 | 0.2277 | 17.65 | 0.60u | 127.02±6.491                                                | 2545.75                                                 | 44.20                                                          | 7.33                        | -0.31           |
| 17 | J222055.73-075317.9 | 0.1489 | 17.60 |       | 188.47±7.977                                                | 2916.25                                                 | 43.87                                                          | 8.02                        | -1.33           |
| 18 | J102914.87+572353.7 | 0.1885 | 17.79 | 0.53u | 256.27±3.611                                                | 2312.89                                                 | 43.99                                                          | 8.56                        | -1.75           |
| 19 | J094859.47+433518.9 | 0.2262 | 16.91 | 0.16u | 150.49±2.132                                                | 2294.98                                                 | 44.49                                                          | 7.63                        | -0.32           |
| 20 | J100756.46+491809.5 | 0.1496 | 17.98 | 0.60u | 103.85±4.431                                                | 2252.58                                                 | 43.73                                                          | 6.98                        | -0.43           |
| 21 | J095744.43+075124.8 | 0.1406 | 17.61 | 0.47u | 134.84±5.772                                                | 2594.93                                                 | 43.81                                                          | 7.44                        | -0.81           |
| 22 | J140502.65+470747.5 | 0.1521 | 17.54 | 0.42u | 130.14±5.365                                                | 2782.77                                                 | 43.92                                                          | 7.37                        | -0.63           |
| 23 | J151535.25+480530.5 | 0.3115 | 16.52 | 0.01u | 192.45±6.467                                                | 2980.23                                                 | 44.89                                                          | 8.06                        | -0.35           |
| 24 | J144207.69+384411.3 | 0.1457 | 17.48 | 0.40u | 116.35±2.027                                                | 2643.79                                                 | 43.91                                                          | 7.18                        | -0.45           |
| 25 | J153415.41+303435.4 | 0.0938 | 16.98 | 0.20u | 183.73±2.272                                                | 2940.21                                                 | 43.72                                                          | 7.98                        | -1.44           |
| 26 | J082930.59+081238.0 | 0.1291 | 17.21 | 0.32  | 165.72±1.981                                                | 3005.78                                                 | 43.91                                                          | 7.80                        | -1.07           |

Notes: The first Column lists the ID number of the object. The second and third Columns present the name in the format of “SDSS Jhhmmss.ss±ddmmss.s” and redshift of each object. The fourth column presents the PSF magnitude in  $r$  band of SDSS. The fifth column gives the value of  $R_r$  (radio loudness) as defined by Ivezić et al. (2002), ‘u’ represents the value of an upper limit one. The following two columns list the line width of [NII] $\lambda$ 6583Å and broad H $\alpha$  in units of  $\text{km} \cdot \text{s}^{-1}$ . The last three columns contain the value of continuum luminosity at 5100 Å (corrected for Galactic extinction including the reddening correction, following Schlegel et al. 1998), the value of BH masses estimated from the line width of [OIII] $\lambda$ 5007Å (as a tracer of velocity dispersion) and the dimensionless accretion rate of the dbp emitters.

The line width of broad H $\alpha$  of J2125-0813 is estimated from the linewidth of broad H $\beta$  produced by the accretion disk model. Here, we just list the PSF magnitude at  $r$  band for each object.

results indicate that the anti-correlation between  $\text{EW}(\text{FeII})/\text{EW}(\text{H}\beta)$  and line width of broad lines is also valid for dbp emitters.

The correlation between FeII properties and the line width of Balmer broad lines reflects, to some extent, effects of the line of sight. In the case of the correlation between the FeII properties and the width of

the narrow lines, which are considered as tracers of stellar velocity dispersion, the effect of the bulge-BH mass on the properties of FeII emission may be more neatly deconvolved. A detailed description about this is shown in the next subsection. Figure 5 shows the correlation between  $\text{EW}(\text{FeII})/\text{EW}(\text{H}\beta)$  and line width of narrow lines. Here, we select the line width

TABLE 2  
PARAMETERS OF THE ACCRETION DISK MODEL

| Id | $r_{in}$<br>R <sub>g</sub> | $r_{out}$<br>R <sub>g</sub> | $i$  | $e$       | $q$       | $\sigma$<br>km·s <sup>-1</sup> | $k_{H\beta}$ | $k_{FeII}$ |
|----|----------------------------|-----------------------------|------|-----------|-----------|--------------------------------|--------------|------------|
| 0  | 991                        | 4054                        | 33   | 0.25      | 2.57      | 2032±754                       | 0.39         | 0.35       |
| 1  | 391±62                     | 4085±151                    | 89±6 | 0.26±0.01 | 0.98±0.11 | 738±90                         | 0.40         | 0.28       |
| 2  | 385                        | 969                         | 28   | 0.57      | 3.61      | 2059±400                       | 0.43         | 0.13       |
| 3  | 367±37                     | 11946±1077                  | 50±3 | 0.24±0.01 | 1.71±0.01 | 296±25                         | 0.37         | 0.11       |
| 4  | 37±17                      | 2660±158                    | 26±1 | 0.21±0.01 | 1.29±0.02 | 700±43                         | 0.39         | 0.18       |
| 5  | 526±89                     | 5557±833                    | 54±5 | 0.21±0.01 | 1.29±0.08 | 771±60                         | 0.47         | 0.21       |
| 6  | 526±21                     | 3350±255                    | 89   | 0.96±0.01 | 2.24±0.05 | 703±48                         | 0.36         | 0.41       |
| 7  | 103±3                      | 1804±29                     | 21±0 | 0.27±0.02 | 1.21±0.01 | 915±21                         | 0.36         | 0.10       |
| 8  | 2797                       | 32768                       | 89   | 0.17      | 7.40±1.86 | 1622±275                       | 0.54         | 0.27       |
| 9  | 210±112                    | 5705                        | 47   | 0.03      | 1.43±0.20 | 1813±1078                      | 0.34         | 0.42       |
| 10 | 394±40                     | 4953±142                    | 89   | 0.24±0.01 | 0.97±0.07 | 1238±55                        | 0.34         | 0.35       |
| 11 | 31±6                       | 339±40                      | 15±1 | 0.01      | 1.58±0.19 | 2610±270                       | 1.00         | 0.53       |
| 12 | 222±18                     | 3382±374                    | 85±2 | 0.90±0.01 | 2.03±0.04 | 624.6±46.5                     | 0.45         | 0.44       |
| 13 | 30±8                       | 12790±507                   | 25±0 | 0.33±0.01 | 1.56±0.01 | 292±13                         | 0.42         | 0.38       |
| 14 | 408±11                     | 3100±116                    | 86±1 | 0.94±0.01 | 2.15±0.02 | 562.5±40.5                     | 0.51         | 0.42       |
| 15 | 578±340                    | 32768                       | 72   | 0.26±0.08 | 1.36±0.01 | 479±16                         | 0.36         | 0.47       |
| 16 | 208±12                     | 4830±333                    | 85±2 | 0.84±0.01 | 1.85±0.02 | 499±24                         | 0.44         | 0.36       |
| 17 | 11±1                       | 7779±428                    | 30±0 | 0.23±0.01 | 1.44±0.01 | 476.4±33.30                    | 0.54         | 0.65       |
| 18 | 23±13                      | 6843±387                    | 23±0 | 0.34±0.01 | 1.54±0.03 | 461.4±27.00                    | 0.53         | 0.40       |
| 19 | 88±7                       | 3401±226                    | 89±2 | 0.84±0.01 | 1.46±0.02 | 572.7±21.30                    | 0.41         | 0.52       |
| 20 | 406±30                     | 4875±346                    | 84±7 | 0.87±0.01 | 1.92±0.04 | 451.5±32.40                    | 0.51         | 0.53       |
| 21 | 141±43                     | 26691±4774                  | 54±7 | 0.28±0.01 | 1.50±0.01 | 429.6±23.70                    | 0.30         | 0.23       |
| 22 | 99±19                      | 15609±1578                  | 44±2 | 0.32±0.01 | 1.63±0.01 | 303.9±23.70                    | 0.51         | 0.75       |
| 23 | 104±16                     | 13542±1252                  | 41±2 | 0.33±0.01 | 1.73±0.01 | 461.7±27.30                    | 0.54         | 0.42       |
| 24 | 99±13                      | 2551±278                    | 78±1 | 0.81±0.01 | 1.54±0.03 | 566.1±22.80                    | 0.50         | 0.40       |
| 25 | 307±24                     | 21499±1118                  | 81±8 | 0.28±0.01 | 1.56±0.01 | 352.2±22.50                    | 0.44         | 0.42       |
| 26 | 77±6                       | 2285±150                    | 76±8 | 0.83±0.01 | 1.71±0.02 | 676.8±29.10                    | 0.39         | 0.36       |

Notes: If the error of the parameter is larger than the value of the parameter, we do not show the error. The id number represents the name in the Table 1.

of the [OIII] emission line. As described above, two Gaussian components are needed for [OIII] emission line: one normal (core) component and an extended one. We use the core components as described in Greene & Ho (2005a). The Spearman rank of the correlation coefficient is  $-0.52$  with  $P_{null} \sim 0.6\%$ .

Moreover, we check the correlation between EW(FeII) and the ratio of the peak height of [OIII] $\lambda 5007\text{\AA}$  to that of H $\beta$  (peak  $\lambda 5007\text{\AA}$ ) as described by Boroson & Green (1992). The correlation between EW(FeII) and peak  $\lambda 5007\text{\AA}$  discovered by Boroson & Green (1992) using a sample of low redshift quasars is confirmed for dbp emitters. The Spearman rank correlation coefficient is  $-0.24$  with

$P_{null} \sim 3\%$ . The plot is shown in Figure 6. The result indicates that the parameter, peak  $\lambda 5007\text{\AA}$ , is a better indicator of dbp emitters with strong FeII emission lines.

Furthermore, we check the radio properties of dbp emitters with apparent FeII emission lines. We find that there are 8 dbp emitters in our sample targeted and 13 dbp emitters covered by FIRST/NVSS. Thus, we can get the radio flux density or the upper limit value of radio flux density at 20cm. According to the definition of radio loudness,  $R_i$ , by Ivezić et al. (2002):

$$R_i = \log(F_{20cm}/F_i) = 0.4 \times (m_i - t) \quad (2)$$

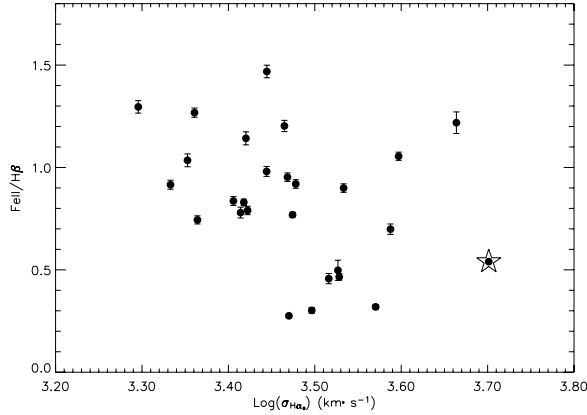


Fig. 4. The correlation between  $EW(\text{FeII})/EW(\text{H}\beta)$  and the line width of broad  $\text{H}\alpha$ . The five-point star represents the object SDSS J2125-0813.

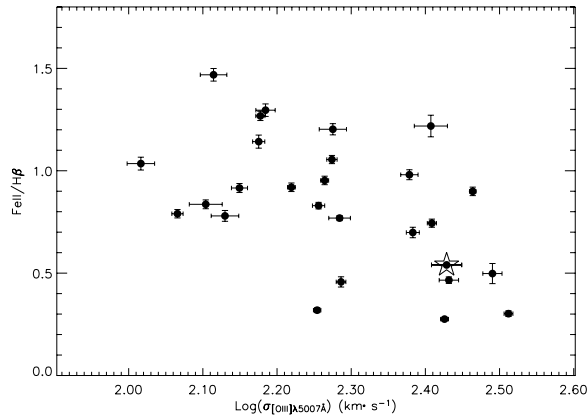


Fig. 5. The correlation between  $EW(\text{FeII})/EW(\text{H}\beta)$  and the line width of  $[\text{OIII}]\lambda 5007\text{\AA}$ . The five-point star represents the object SDSS J2125-0813.

where  $m_i$  is one of the SDSS magnitudes and  $t$  is the 20cm AB radio magnitude defined as  $t = -2.5 \log(F_{20\text{cm}}/3631\text{Jy})$ , we can calculate radio loudness for each dbp emitter in our sample. There is only one dbp emitter with  $R_r > 1$ , SDSS J075407.95+431610.5, which is a radio loud quasar. The other 20 dbp emitters are radio quiet quasars. Thus dbp emitters with stronger FeII emission lines are apt to be found in radio quiet quasars, which is in agreement with the E1 analysis of single peaked BRL AGN (e.g. Sulentic et al. 2003).

It is also convenient to check the correlation between the continuum luminosity and the luminosity of  $\text{H}\alpha$ , which is confirmed by Greene & Ho (2005b) using a sample of AGN selected from SDSS, because in our code the flux of  $\text{H}\alpha$  is one of fundamental parameters to determine the flux of other

emission lines, such as the flux of double-peaked  $\text{H}\beta$ ,  $k_{\text{H}\beta} \times f_{\text{H}\alpha}$ , the flux of FeII emission lines, and  $K_{\text{FeII}} \times f_{\text{H}\alpha}$ . One of the main considerations is that the correlation reflects some physical parameters of BLRs of AGN, such as the covering factor of BLRs, the proportional contribution of the ionization energy to the emission of broad emission lines, etc. The correlation is shown in Figure 7. The Spearman rank correlation coefficient is  $\sim 1$  with  $P_{\text{null}} \sim 0$ . The correlation for dbp emitters obeys the same relation as that for normal AGN,  $L_{\text{H}\alpha} \sim L_{5100\text{\AA}}^{1.157}$ . Here, the luminosity of  $\text{H}\alpha$  also includes the contributions of [NII] doublets, besides the contributions of broad and narrow components of  $\text{H}\alpha$ , because sometimes it is difficult to separate the narrow component of  $\text{H}\alpha$  from the components of [NII] for some dbp emitters. Because of the small contributions of [NII] emission lines, the relation between  $L_{\text{H}\alpha}$  and  $L_{5100\text{\AA}}$  is not affected.

In the case of dbp we can get, from the best fitted results of the accretion disk model, the inclination angle of the accretion disk. The plot of the strength of FeII vs. the inclination angle of the accretion disk is shown in Figure 8. The Spearman Rank correlation coefficient is 0.43 with  $P_{\text{null}} \sim 6\%$ . We selected only 20 objects with accurate inclination angles  $i$ ,  $i > 1.5 \times i_{\text{error}}$ . The inclination angle derived from the accretion disk model has a somewhat large error, specially when the angle is near 90 degrees. We cannot confirm a trend for all objects, because if we only consider the objects with inclination angle less than 60 degrees the coefficient is 0.16 with  $P_{\text{null}} \sim 63\%$ . On the other hand, if the trend between the strength of FeII emission lines and the inclination angle shown in Figure 7 were true, it would indicate that the objects with broader Balmer lines have stronger FeII emission lines, which is in contradiction with the much stronger correlation between strength of FeII emission lines and line width of broad  $\text{H}\alpha$ . It is also in contradiction with all previous results found from E1 parameter space analysis, e.g. Sulentic et al. (2000). Thus, the trend most be a fake one. This is due not only to the fact that values for the inclination have large errors for large angles, but also to the fact that inclination alone cannot govern the FeII strength, it is always convolved with BH mass and accretion rate, as discussed below (see also Marziani et al. 2003a)

### 3.3. Influence of Black Hole Mass and Accretion Rate

The most accurate way to estimate the central BH masses is by the stellar velocity dispersion as in



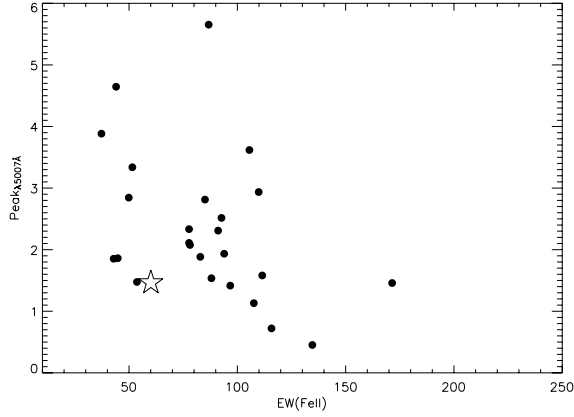


Fig. 6. The correlation between EW(FeII) and the height ratio of [OIII] $\lambda$ 5007Å to that of H $\beta$ . The five-point star represents the object SDSS J2125-0813.

Gebhardt et al. (2000); Ferrarese & Merritt (2001); Tremaine et al. (2002). For quasars, it is not possible to determine the BH masses by the stellar velocity dispersion. Another convenient way is under the assumption of virialization (Greene & Ho 2005b; Ovcharov, Ivanov, & Nedialkov 2005; Wu et al. 2004; McLure & Jarvis 2004; 2002; Marziani, Dultzin-Hacyan, & Sulentic 2006; Onken et al. 2004; Peterson et al. 2004). However, there are various caveats for the measurement of the full width at half maximum (FHHM) of broad low-ionization emission lines, such as H $\beta$ , especially for dbp emitters. A detailed discussion of the line components that do reverberate can be found in Sulentic et al. (2006). Actually, these authors prefer to use the FeII lines (assuming they are virialized as we prove here to determine BH masses). Unfortunately, for double-peaked broad emission lines, it is not reasonable to fit the line by one Gaussian function or to measure the value of FWHM for double-peaked emission lines.

However, there is a strong correlation between stellar velocity dispersion and line width of low-ionization narrow emission lines, which has been studied by many authors for different kinds of AGN. Nelson & Whittle (1996) found that there is a correlation between line width of [OIII] $\lambda$ 5007Å and stellar velocity dispersion. Wang & Lu (2001) also emphasized the relation for a sample of NLS1s. Recently, Greene & Ho (2005a) confirmed that the line width of low-ionization narrow emission lines can trace the stellar velocity dispersion using a sample of low luminous AGN selected from SDSS (York et al. 2000; Strauss et al. 2002; Abazajian et al. 2004). Zhou et al. (2006) re-confirmed the stronger relation for

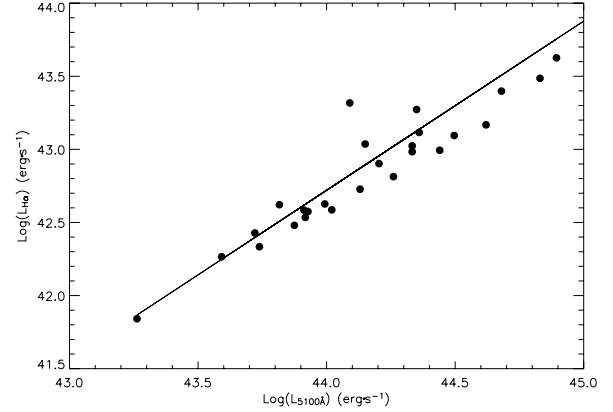


Fig. 7. The correlation between the continuum luminosity and the luminosity of H $\alpha$ .

a larger sample of NLSy1 selected from SDSS by line width of [NII] emission line. As a test, Boroson (2003) has shown the coincidence between the BH masses estimated from the relation  $M_{BH} - \sigma_{[OIII]}^{4.02}$  and the BH masses estimated under the assumption of virialization for a sample of AGN selected from SDSS.

As mentioned above, in order to determine the BH masses of the dbp emitters, we use the line width of [OIII] emission line as the estimator, according to the following equation (Gebhardt et al. 2000; Ferrarese & Merritt 2001; Tremaine et al. 2002):

$$M_{BH} = 10^{8.13 \pm 0.06} \left( \frac{\sigma_{[OIII]}}{200 \text{ km} \cdot \text{s}^{-1}} \right)^{4.02 \pm 0.32} M_{\odot} \quad (3)$$

where  $\sigma_{[OIII]}$  is the line width of the normal component of [OIII] $\lambda$ 5007Å. The correlation between BH masses and EW(FeII)/EW(H $\beta$ ) has been pointed out above as the correlation between  $\sigma_{[OIII]\lambda 5007\text{\AA}}$  and EW(FeII)/EW(H $\beta$ ) (Figure 5) The anti-correlation of EW(FeII)/EW(H $\beta$ ) and line width of [OIII] $\lambda$ 5007Å indicates that the dbp emitters with lower BH masses have stronger FeII emissions. This result is in agreement with that of E1 analysis of single peaked BRL AGN (e.g. Sulentic et al. 2000).

The correlation between the dimensionless accretion rate and EW(FeII)/EW(H $\beta$ ) is shown in Figure 9. The dimensionless accretion rate  $\dot{m}$  is calculated as  $\dot{m} = 9 \times L_{5100\text{\AA}} / M_{BH} \times 1.38 \times 10^{38}$  (Wandel, Peterson, & Malkan 1999; Kaspi et al. 2000). The Spearman rank correlation coefficient is 0.23 with  $P_{null} \sim 24\%$ . Such a weak correlation indicates that dimensionless accretion rate has weaker effects on FeII emission of dbp emitters than does the BH mass.

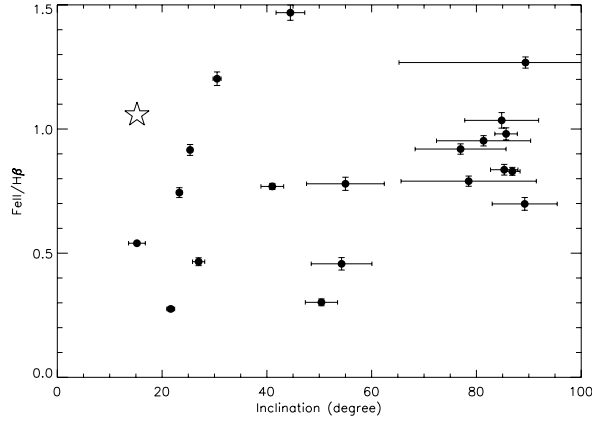


Fig. 8. The correlation between  $EW(\text{FeII})/EW(\text{H}\beta)$  and the inclination angle of the accretion disk. The five-point star represents the object SDSS J2125-0813.

The mean BH masses for the 27 dbp emitters is  $10^{8.05 \pm 0.11} M_{\odot}$ , the mean dimensionless accretion rate is  $10^{-1.04 \pm 0.11}$ . According to the dimensionless accretion rate, the accretion mode in the central region is standard accretion rather than ADAF mode, because the upper limit accretion rate for ADAF mode is about  $\dot{m} \sim 0.28 \times \alpha^2$  where  $\alpha$  is viscous coefficient  $\alpha \sim 0.1 - 0.3$  (Mahadevan & Quataert, 1997; Lasota et al. 1996; Narayan, Yi, & Mahadevan 1995). If we select  $\alpha \sim 0.1$  (Yi, 1996; Choi, Yang, & Yi 2001), all the dbp emitters in our sample have larger accretion rates than the critical value 0.0028. Furthermore, the 27 dbp emitters have normal quasar spectra, with normal big blue bumps. Thus, even if ADAF accretion mode dominates the accretion flow in the inner region of the accretion disk, especially for the two objects with lower accretion rate, the standard accretion mode should mainly dominate the bulk of accretion.

#### 4. DISCUSSIONS AND CONCLUSIONS

We have accurately reproduced the line profiles in the wavelength range from 4100 Å to 5600 Å by the line profile of double-peaked broad  $\text{H}\alpha$ . The best fitted results indicate that the broad optical FeII emission lines are also double-peaked and originate from the same place where the double-peaked broad Balmer emission lines. More and more evidence confirms that the double-peaked broad low-ionization lines come from the accretion disk rather than from an outflow or other models. In our sample, the double-peaked broad  $\text{H}\alpha$  of all the 27 dbp emitters can be best fitted by the elliptical accretion disk model (Eracleous et al. 1995). The best

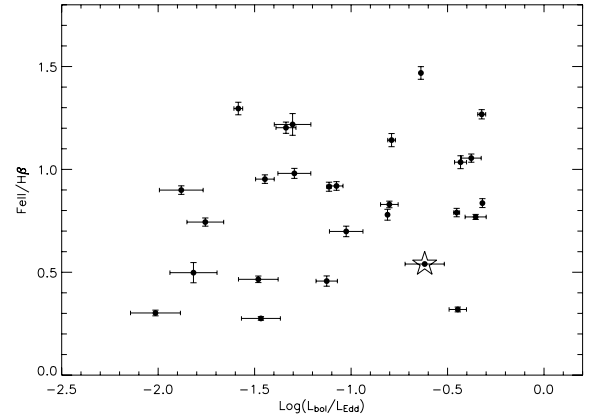


Fig. 9. The correlation between accretion rate and  $EW(\text{FeII})/EW(\text{H}\beta)$ . The five-point star represents the object SDSS J2125-0813.

fitted results for the optical FeII emission lines indicate that the FeII emission lines also originate from the accretion disk which provides the needed high density for these lines.

The accretion rate and the normal quasar spectra indicate that ADAF accretion mode in the dbp emitters with FeII emission lines is not the main accretion mode. BH masses have more influence on the FeII properties of dbp emitters than the dimensionless accretion rate. The reliable anti-correlation between  $EW(\text{FeII})/EW(\text{H}\beta)$  and  $\sigma_{\text{H}\alpha}$  indicates that for dbp emitters the emission region of stronger FeII lines are far from the central black hole. We have shown that even for dbp emitters the influence of orientation on FeII intensity cannot be deconvolved from the other determining physical parameters of these AGN: mainly BH mass and, to a lesser extent, accretion rate.

We also obtain the same strong correlation between  $L_{5100\text{\AA}}$  and  $L_{\text{H}\alpha}$  (including the broad and narrow components near  $\text{H}\alpha$ ) for dbp emitters in our sample as that obeyed by normal AGN, which indicates that the connection between the continuum and BLRs is the same for normal AGN and for dbp emitters. We know that the luminosity of broad emission lines, such as broad  $\text{H}\alpha$ , can be estimated as  $L_{\text{H}\alpha} = h\nu_{\text{H}\alpha} n_e n_{\text{H}} \alpha_{\text{H}\alpha} \epsilon V$ , where  $\alpha_{\text{H}\alpha}$  is the recombination coefficient for  $\text{H}\alpha$ , and  $\epsilon V$  is the volume filled by gas in BLRs. The electron density in the accretion disk is larger than that in the normal BLRs, which indicates that the value of  $n_e n_{\text{H}} \alpha_{\text{H}\alpha} \epsilon V$  is a constant for AGN, normal AGN and dbp emitters.

Finally we want to stress that the correlations, or more precisely perhaps, the trends pointed out above

remain to be confirmed, because of two main reasons: first, the comparative numbers of well defined dbp emitters is small (which is intriguing enough), and second, because one of our selection criteria (the apparent strength of optical FeII) may bias the trends.

ZXG gratefully acknowledges the postdoctoral scholarships offered by Universidad Nacional Autónoma de México (UNAM). D. D-H acknowledges support from grant IN100703 from DGAPA, UNAM. This research has made use of the NASA/IPAC Extragalactic Database (NED) which is operated by the Jet Propulsion Laboratory, California Institute of Technology, under contract with the National Aeronautics and Space Administration. This paper has also made use of the data from the SDSS projects. Funding for the creation and the distribution of the SDSS Archive has been provided by the Alfred P. Sloan Foundation, the Participating Institutions, the National Aeronautics and Space Administration, the National Science Foundation, the U.S. Department of Energy, the Japanese Monbukagakusho, and the Max Planck Society. The SDSS is managed by the Astrophysical Research Consortium (ARC) for the Participating Institutions. The Participating Institutions are The University of Chicago, Fermilab, Institute for Advanced Study, Japan Participation Group, The Johns Hopkins University, Los Alamos National Laboratory, Max-Planck-Institute for Astronomy (MPIA), Max-Planck-Institute for Astrophysics (MPA), New Mexico State University, Princeton University, United States Naval Observatory, and University of Washington.

#### REFERENCES

- Abazajian, K., et al. 2004, *AJ*, 128, 502
- Antonucci, R., Hurt, T., & Agol, E. 1996, *ApJ*, 456, 25
- Baldwin, J. A., Ferland, G. F., Korista, K. T., Hamann, A., & LaCluyze, A. 2004, *ApJ*, 615, 610
- Baldwin, J. A., Ferland, G. F., Korista, K. T., & Verner, D. 1995, *ApJ*, 455, L119
- Begelman, M. C., Blandford, R. D., & Rees, M. J. 1980, *Nature*, 287, 307
- Bergeron, J., & Knuth, D. 1980, *A&A*, 85, L11
- Boroson, T. A. 2003, *ApJ*, 584, 647
- Boroson, T. A., & Green, R. F. 1992, *ApJS*, 80, 109
- Bottoff, M., Ferland, G., Baldwin, J., & Korista, K. 2000, *ApJ*, 542, 644
- Chen, K. Y., & Halpern, J. P. 1989a, *ApJ*, 344, 115
- Chen, K. Y., Halpern, J. P., & Filippenko, A. V. 1989b, *ApJ*, 339, 742
- Chen, K. Y., Halpern, J. P., & Titarchuk, L. G. 1997, *ApJ*, 483, 194
- Choi, Y.-Y., Yang, J., & Yi, I. 2001, *ApJ*, 555, 673
- Collin-Souffrin, S., Hameury, J. M., & Joly, M. 1988, *A&A*, 205, 19
- Collin-Souffrin, S., Joly, M., Péquignot, D., & Dumont, S. 1986, *A&A*, 166, 27
- Dumont, A. M., Collin-Souffrin, S., & Nazarova, L. 1998, *A&A*, 331, 11
- Eracleous, M., & Halpern, J. P. 1994, *ApJS*, 90, 1
- \_\_\_\_\_. 2003, *ApJ*, 599, 886
- Eracleous, M., Halpern, J. P., Gilbert, A. M., Newman, J. A., & Filippenko, A. V. 1997, *ApJ*, 490, 216
- Eracleous, M., Livio, M., Halpern, J. P., & Storchi-Bergmann, T. 1995, *ApJ*, 438, 610
- Ferland, G. J., & Person, S. E. 1989, *ApJ*, 347, 656
- Ferrarese, L., & Merritt, D. 2001, *MNRAS*, 320, L30
- Francis, P. J., Hewett, P. C., Foltz, C. B., Chaffee, F. H., Weymann, R. J., & Morris, S. L. 1991, *ApJ*, 373, 465
- Gaskell, C. M. 1983, *Nature*, 304, 212
- Gebhardt, K., et al. 2000, *ApJ*, 439, L13
- Gilbert, A. M., Eracleous, M., Filippenko, A. V., & Halpern, J. P. 1999, *BAAS*, 31, 950
- Grandi, S. A. 1981, *ApJ*, 251, 451
- \_\_\_\_\_. 1982, *ApJ*, 255, 25
- Greene, J. E., & Ho, L. C. 2005a, *ApJ*, 627, 721
- \_\_\_\_\_. 2005b, *ApJ*, 630, 12
- Halpern, J. P., Eracleous, M., Filippenko, A. V., & Chen, K. Y. 1996, *ApJ*, 464, 704
- Hao, L., et al. 2005, *AJ*, 129, 1783
- Hartnoll, S. A., & Blackman, E. G. 2002, *MNRAS*, 332, L1
- Ivezić, Z., et al. 2002, *AJ*, 124, 2364
- Joly, M. 1987, *A&A*, 184, 33
- \_\_\_\_\_. 1991, *A&A*, 242, 49
- Karas, V., Martocchia, A., & Subr, L. 2001, *PASJ*, 53, 189
- Kaspi, S., Smith, P. S., Netzer, H., Maoz, D., Jannuzi, B., & Giveon, U. 2000, *ApJ*, 533, 631
- Korista, K., Baldwin, J., Ferland, G., & Verner, D. 1997, *ApJS*, 108, 40
- Kwan, J., Cheng, F.-Z., Fang, L.-Z., Zheng, W., & Ge, J. 1995, *ApJ*, 440, 628
- Laor, A., Jannuzi, B. T., Green, R. F., & Boroson, T. A. 1997, *ApJ*, 489, 656
- Lasota, J. P., Abramowicz, M. A., Chen, X., Krolik, J., Narayan, R., & Yi, I. 1996, *ApJ*, 462, 142L
- Li, C., Wang, T. G., Zhou, H. Y., Dong, X. B., & Cheng, F. Z. 2005, *AJ*, 129, 669
- Mahadevan, R., & Quataert, E. 1997, *ApJ*, 490, 605
- Marziani, P., Dultzin-Hacyan, D., & Sulentic, J. W. 2006, *New Developments in Black Hole Research* (New York: Nova Science Publisher Inc.)
- Marziani, P., Sulentic, J. W., Zamanov, R., Calvani, M., Dultzin-Hacyan, D., Bachev, R., & Zwitter, T. 2003a, *ApJS*, 145, 199
- Marziani, P., Zamanov, R., Sulentic, J. W., Dultzin-Hacyan, D., Bongardo, C., & Calvani, M. 2003b, in *ASP Conf. Ser. 290, Active Galactic Nuclei: From Center Engine to Host Galaxy*, ed. S. Collin,

- F. Combes, & I. Shlosman (San Francisco: ASP), 229
- McLure, R. J., & Jarvis, M. J. 2002, *MNRAS*, 337, 109
- \_\_\_\_\_. 2004, *MNRAS*, 353, 45
- Moore, C. E., & Merrill, P. W. 1968, in *NSRDS-NBS 23, Partial Grotrian Diagrams of Astrophysical Interest* (Washington: US Government Printing Office)
- Narayan, R., Yi, I., & Mahadevan, R. 1995, *Nature*, 374, 623
- Nelson, C. H., & Whittle, M. 1996, *ApJ*, 465, 96
- Netzer, H. 1985, *ApJ*, 289, 451
- \_\_\_\_\_. 1988, in *IAU Colloq. 94, Physics of Formation of FeII Lines outside LTE*, ed. R. Viotti, A. Vittone, & M. Friedjung (Dordrecht: Reidel), 247
- Oke, J. B., & Lauer, T. R. 1979, *ApJ*, 230, 360
- Onken, C. A., Ferrarese, L., Merritt, D., Peterson, B. M., Pogge, R. W., Vestergaard, M., & Wandel, A. 2004, *ApJ*, 615, 645
- Ovcharov, E., Ivanov, V. D., & Nedialkov, P. 2005, in *Growing Black Holes: Accretion in a Cosmological Context*, *ESO Astrophysics Symposia*, ed. A. Merloni, S. Nayakshin, & R. A. Sunyaev (Berlin: Springer), 134
- Penston, M. V. 1988, *MNRAS*, 233, 601
- Peterson, B. M., et al. 2004, *ApJ*, 613, 682
- Phillips, M. M. 1978, *ApJ*, 226, 736
- \_\_\_\_\_. 1979, *ApJS*, 39, 377
- Schlegel, D., Finkbeiner, D. P., & Davis, M. 1998, *ApJ*, 500, 525
- Shapovalova, A. I., et al. 2001, *A&A*, 376, 775
- Sigut, T. A., & Pradhan, A. K. 1998, *ApJ*, 499, L139
- \_\_\_\_\_. 2003, *ApJS*, 145, 15
- Storchi-Bergmann, T., Baldwin, J. A., & Wilson, A. S. 1993, *ApJ*, 410, L11
- Storchi-Bergmann, T., Eracleous, M., Livio, M., Wilson, A., Filippenko, A., & Halpern, J. 1995, *ApJ*, 443, 617
- Storchi-Bergmann, T., Eracleous, M., Ruiz, M., Livio, M., Wilson, A., & Filippenko, A. 1997, *ApJ*, 489, 87
- Storchi-Bergmann, T., et al. 2003, *ApJ*, 598, 956
- Strateva, I. V., et al. 2003, *AJ*, 126, 1720
- Strauss, M., et al. 2002, *AJ*, 124, 1810
- Sulentic, J. W., Marziani, P., & Dultzin-Hacyan, D. 2000, *ARA&A*, 38, 521
- Sulentic, J. W., Repetto, P., Stirpe, G. M., Marziani, P., Dultzin-Hacyan, D., & Calvani, M. 2006, *A&A*, 456, 926
- Sulentic, J. W., Zamfi, S., Marziani, P., Bachev, R., Calvani, M., & Dultzin-Hacyan, D. 2003, *ApJ*, 597, L17
- Sulentic, J. W., Zheng, W., Calvani, M., & Marziani, P. 1990, *ApJ*, 355, 15
- Tremaine, S., et al. 2002, *ApJ*, 574, 740
- Vanden Berk, D. E., et al. 2001, *AJ*, 122, 549
- Verner, E. M., Verner, D. A., Korista, K. T., Ferguson, J. W., Hamann, F., & Ferland, G. J. 1999, *ApJS*, 120, 101
- Wandel, A., Peterson, B. M., & Malkan, M. A. 1999, *ApJ*, 526, 579
- Wang, T. G., & Lu, Y. J. 2001, *A&A*, 377, 52
- Wills, B. J., Netzer, H., Uomoto, A. K., & Wills, D. 1980, *ApJ*, 237, 319
- Wills, B. J., Netzer, H., & Wills, D. 1980, *ApJ*, 241, L1
- Wu, X. B., Wang, R., Kong, M. Z., Liu, F. K., & Han, J. L. 2004, *A&A*, 424, 793
- Yi, I. 1996, *ApJ*, 473, 645
- York, D. G., et al. 2000, *AJ*, 120, 1579
- Zhang, X.-G., Dultzin-Hacyan, D., & Wang, T.-G. 2006a, *MNRAS*, 372, L5 (Paper I)
- \_\_\_\_\_. 2007, in preparation
- Zheng, W., Kriss, G. A., Telfer, R. C., Grimes, J. P., & Davidsen, A. F. 1997, *ApJ*, 475, 469
- Zheng, W., Sulentic, J. W., & Binette, L. 1990, *ApJ*, 365, 115
- Zhou, H.-Y., Wang, T.-G., Yuan, W., Lu, H., Dong, X., Wang, J., & Lu, Y. 2006, *ApJS*, 166, 128

Deborah Dultzin-Hacyan and Xue-Guang Zhang: Instituto de Astronomía, Universidad Nacional Autónoma de México, Apdo. Postal 70-264, México D. F. 04510, Mexico (deborah, xguang@astroscu.unam.mx).

Ting-Gui Wang: Center for Astrophysics, Department of Astronomy and Applied Physics, University of Science and Technology of China, Hefei, Anhui, P.R. China (twang@ustc.edu.cn).